Properties of Hydrous Oxide Films Formed at Amorphous Ni-Co Alloys

K. K. Lian*,[1] and V. I. Birss**

Chemistry Department, University of Calgary, Calgary, Alberta, T2N 1N4, Canada

ABSTRACT

The properties of hydrous oxide films, formed electrochemically at an amorphous Ni-Co based alloy by a potential cycling technique, have been investigated in alkaline solutions. The principal reaction occurring at these films is the oxidation/reduction of Ni/Co sites between oxidation states. The sweep rate dependence of this reaction for thin oxide films has demonstrated that it is reversible, while for thicker films, the reaction is diffusion-controlled, with the oxidation process being significantly more inhibited, at least initially, than the reduction reaction. The pH dependence of the principal electrochemical reaction is *ca.* 75-85 mV per pH unit, indicative of alkali metal involvement in the reaction, which occurs in order to preserve electroneutrality within the film. Tafel plots for the oxygen evolution reaction, at both oxide-free and oxidized electrodes, have slopes of *ca.* 45 mV, similar to those observed at spinel and Ni oxide electrodes. At an oxide-free electrode, the hydrogen evolution reaction displays a 120-mV Tafel slope, while in the presence of an oxide film, the reaction is completely inhibited at overpotentials up to *ca.* 300 mV. At more negative potentials, the oxide film appears to be reducible, producing an active high-area electrode.

In our previous paper (1), we described the growth behavior of a hydrous oxide film on an amorphous alloy, composed principally of Ni (51 weight percent) and Co (23 weight percent), in alkaline solutions. It was shown that, initially, the application of a moderately positive potential appeared to lead to the loss of an enriched, oxidized Cr layer from the "as-received" alloy surface. After its removal, a hydrous oxide film, exhibiting an electrochemical response similar to that of Ni oxide, could very readily be formed as a consequence of the application of a particular potential cycling regime (between *ca.* 1.5 and 0 V). With continuous cycling (1), a thick film could be developed at the alloy surface, as reflected by the magnitude of the oxidation/reduction peaks centered at *ca.* 1.35 V. It is of interest that, as the oxide film thickened, the rate of the hydrogen evolution reaction (HER) appeared to diminish.

Hydrous oxide films are known to have a number of very useful properties (2-12). Because of their high charge capacity, and their generally rapid charge/discharge kinetics, they are of potential use as cathodes in secondary batteries. Also, oxides formed at metals such as Ru (7), Ir (4, 6), Co (8, 9), etc., are known to be superior electrocatalysts for reactions such as chlorine and oxygen evolution (OER). The electrochromic properties of these oxides have been taken advantage of in display devices (10, 11), and recently, interest has arisen in the application of hydrous Ir oxides (12) as interneural stimulating electrodes.

Therefore, it is of interest to determine the properties of hydrous oxide films formed at alloy electrodes, particularly if more than one electroactive metal is present, and to determine the effect of an amorphous substrate on the properties of hydrous oxides, viewed as being porous and amorphous in nature (6). In addition, it is important to obtain an understanding of the properties of the oxide film formed on these amorphous alloys from the point of view of the potential future use of these materials in aggressive environments. This work provides insight into the probable corrosion behavior of these materials in environments where a local alkaline pH may be encountered.

Experimental

The principal details of the electrochemical experiments and surface analysis techniques utilized in this study of amorphous $Ni_{51}Co_{23}Cr_{10}Mo_7Fe_{5.5}B_{3.5}$ ribbons have been provided in our previous paper (1). In the present work, 1*M* NaOH solutions were utilized in all standard experiments, while less alkaline solutions were composed of NaOH and $NaClO_4$ as the supporting electrolyte. The "as-received" and electrochemically oxidized alloys were also examined in borate-buffered (pH 8.5 to 9.6) NaCl-containing solutions. In addition to cyclic voltammetry, potentiostatic methods were used to investigate the kinetics of the HER and the OER. The corrosion resistance of the amorphous alloy was determined both by slow-sweep cyclic voltammetry and tracking of the open-circuit potential (OCP).

Results and Discussion

Interplay between quantity of oxide and oxidation/reduction kinetics.—The first scan of potential in the range from the HER to the OER shows two anodic peaks and one small cathodic peak (Fig. 1, ——), with the anodic charge greatly exceeding the cathodic one. By analogy to the electrochemical response of the elements composing this amorphous alloy, and from surface and solution analyses, it was shown (1) that Cr (and possibly Mo and B) are dissolving from a surface-enriched region of the alloy in this potential range, primarily in the range of peak A_1 (at *ca.* 1.3 V). The second scan of potential (---) shows that peak A_1 is no longer present, and that a characteristic set of peaks, A_2/C_2, centered at *ca.* 1.35 V, have developed.

Peaks A_2/C_2 are believed to reflect the occurrence of a redox process within a surface oxide film in which the oxidation state of the Ni (and Co) sites increases/decreases by one, similar to the Ni(II)/(III) transformation observed for Ni oxide at polycrystalline Ni electrodes (1). When the potential is scanned repetitively between an upper limit, E_+, of *ca.* 1.5 V, in the range of the OER, and then negatively to a lower limit, E_-, of *ca.* 0 V, peaks A_2/C_2 increase in magnitude, reflecting oxide film growth as a consequence of this potential cycling regime. The charge densities associated with peaks A_2 and C_2, determined after subtraction of the background current of the OER, are very similar, *i.e.*, $Q_a = Q_c$, at all sweep rates investigated.

One very notable feature of the cyclic voltammetric (CV) response of the hydrous oxide film which forms at amorphous Ni-Co alloys after several scans of potential, such as shown in Fig. 1, is the asymmetry in the shape of the anodic and cathodic peaks, A_2/C_2, even when the hydrous oxide film is still very thin. Peak A_2 can be seen to be sharp and narrow (peak width at half-height, $w_{1/2}$ = *ca.* 35 mV), while peak C_2 is substantially broader ($w_{1/2}$ = *ca.* 100 mV) and has a lower peak current than A_2. This is an indication that either the oxide has different properties in the reduced *vs.* oxidized forms and/or that the anodic and cathodic reactions do not involve the same process.

Another striking aspect of the CV behavior is the sweep rate (s) dependence of these two processes. Figure 2 shows an example of this for a relatively thin oxide film which

* Electrochemical Society Student Member.
** Electrochemical Society Active Member.
[1] Department of Metallurgy & Materials Science, University of Toronto, Toronto, Ontario, M5S 1A4, Canada.

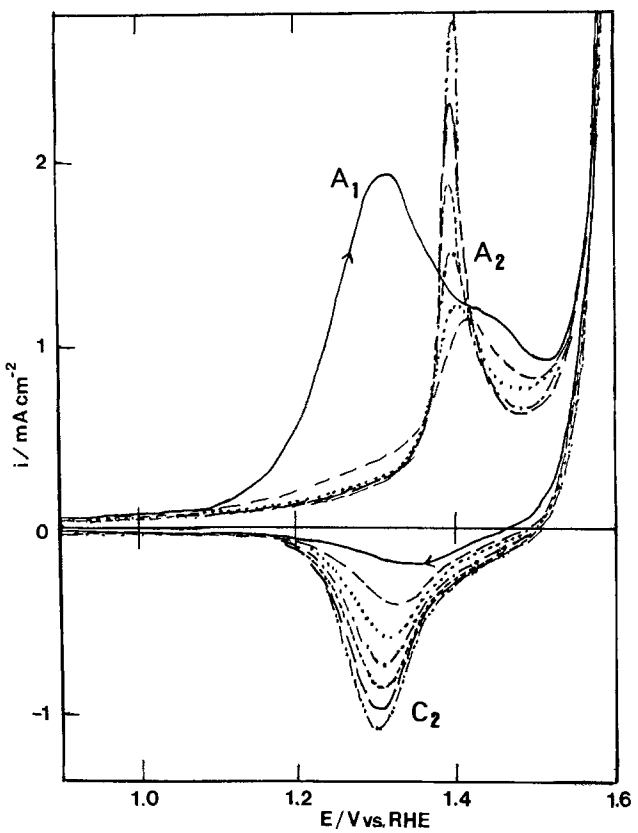

Fig. 1. Electrochemical response of 'as-received' Ni-Co alloy in 1M NaOH, cycles 1 to 7 from −0.2 to 1.6 V; s = 100 mV/s (potential region from −0.2 to 0.9 V not shown in figure).

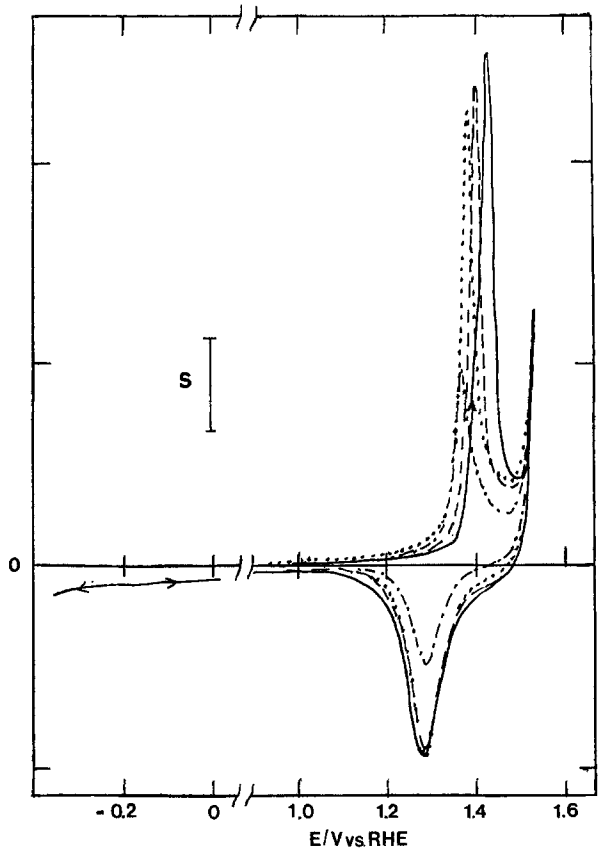

Fig. 2. Dependence of CV response of hydrous Ni-Co oxide (CEF = 18) on sweep rate. s = 5 (— · —), 10 (····), 20 (---), and 50 (——) mV/s. S = 0.18 mA/cm² for s = 5 and 10 mV/s, S = 0.35 mA/cm² for 20 mV/s, and S = 0.7 mA/cm² for s = 50 mV/s.

was formed to a charge enhancement factor (CEF) of 18. The CEF value is calculated from the ratio of the charge density in peaks A_2 (or C_2) after some period of oxide growth, to that observed (*ca.* one monolayer of oxide, 0.15 mC/cm²) in the first cycle of potential of an as-received ribbon sample (1). The CEF value can therefore be considered as a reasonable estimate of the number of monolayers of active oxide material present (1, 7). Clearly, the anodic reaction is more kinetically hindered than the cathodic, as seen by the marked positive shift of the anodic peak with increasing sweep rate, while the cathodic peak shape and potential are essentially unchanged over the range of sweep rates indicated. This is demonstrated more clearly in Fig. 3, which shows that, at slow sweep rates, the anodic peak is located at a substantially more negative potential, although the peak shape difference is still retained. Figure 3 also shows that the positive shift of the anodic peak with sweep rate is greater the thicker the oxide film, while the cathodic peak is hardly affected by film thickness.

Figure 4 demonstrates the dependence of the cathodic peak current density on sweep rate for oxide films of two different thicknesses. In these experiments, the potential was held at E_+ for 10 s before commencing the cathodic sweep to ensure that the film was completely oxidized prior to the reduction step and that only oxide reduction kinetics were being examined. It was not possible to accurately determine the sweep rate dependence of the peak current density for A_2, due to its shift into the region of the OER with increasing sweep rate and the consequent difficulties in baseline determination, particularly for thick oxide films. Figure 4 (left) indicates that thin films show a linear sweep rate dependence, one of the important and unusual characteristics of many hydrous oxide films (3, 7), to higher sweep rates than do thicker oxide films (Fig. 4, right). In fact, at higher sweep rates, an $s^{1/2}$ dependence (Fig. 5), typical for mass transport-limited reactions, is seen.

Strong similarities exist between the results described above and those encountered with particular polymer-coated electrodes, for which electron injection/expulsion during reduction/oxidation is believed to occur by a site-to-site electron hopping mechanism, with associated ion transport to maintain electroneutrality within the polymer film (13-19). When the rate of charge transport through these polymer films is rapid relative to the perturbation rate (*i.e.*, sweep rate), the film oxidation/reduction process obeys the Nernst equation at all potentials, and a linear peak current/sweep rate relationship is obtained (14, 15, 20-22). However, if either electron or ion transport is slow, then a diffusion-limited response is expected and a linear dependence on $s^{1/2}$ should be observed. This argument can be extended to the oxidation/reduction of the hydrous oxide films formed at these Ni-Co alloys, at which a reaction such as [1] can be suggested

$$x\mathrm{OH}^- + \mathrm{Ni(II)Co(III)oxide} \leftrightarrow \mathrm{Ni(III)Co(IV)oxide} + 2e^- \quad [1]$$

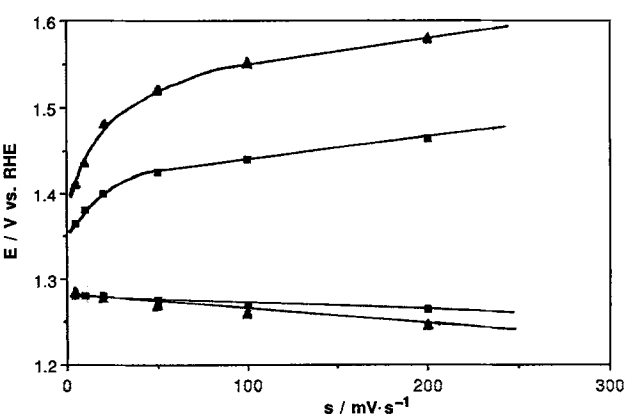

Fig. 3. Dependence of A_2 and C_2 peak potentials on sweep rate. CEF = 8 (■) and 97 (▲).

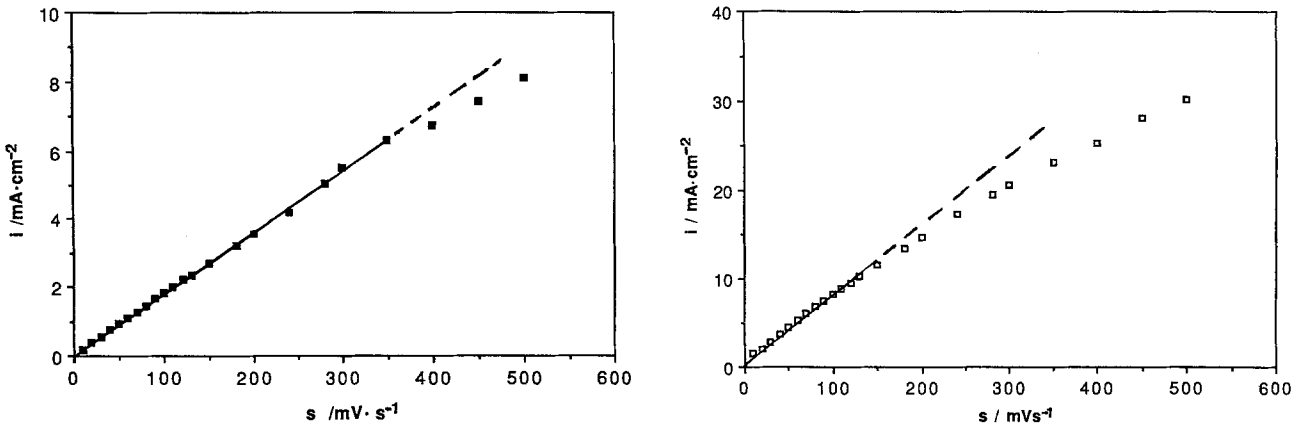

Fig. 4. Dependence of peak current density of C_2 on sweep rate for oxide films of (left) CEF = 8 and (right) CEF = 97.

As will be shown below, x is not necessarily equal to two (when considering two metal sites, as in Eq. [1]), in which case, other charge-compensating ions are required in the overall reaction (see below).

In relation to the above analogy with polymer films at thin oxide films, charge transport is rapid and a linear current/sweep rate relationship is observed, while for thicker oxide films, either electron-hopping into or ion diffusion out of the oxide film could be rate-limiting during oxide reduction. In the latter case, the diffusion coefficient of the rate limiting species, D, can be determined from the slope of the plot in Fig. 5. The semi-infinite linear diffusion equation is therefore applied, as follows

$$i_p = (2.69 \times 10^5)\, n^{3/2} D^{1/2} C s^{1/2} \quad [2]$$

where n is assumed to be 1 [one electron per metal site, *i.e.*, (Ni(III)/(IV) and/or Co(III/IV) transition] and C is the concentration of electroactive sites within the film (mol/cm^3). Here, C can be estimated from the charge, Q, measured in peak C_2 (or A_2) in a slow sweep experiment, *e.g.*, at 5 or 10 mV/s, and from the film volume, V, which can be obtained as a product of the electrode area and the film thickness, determined from SEM examinations (1, 7, 23). It should be noted that Q is considered to be an accurate indicator of the number of reacting metal (Ni, Co) sites within the film, as it is independent of sweep rate and as there is no evidence for the occurrence of any other concurrent reactions. Thus

$$C = Q/(nFV) \quad [3]$$

For the data plotted in Fig. 5, where Q is 5.5×10^{-3} C and the film thickness is *ca.* 90 nm, $D = 1.9 \times 10^{-10}$ cm^2/s. Although there are numerous approximations involved in this calculation, this value is very similar to those obtained for mass-transport-limited charge transfer through the polymer-modified electrodes referred to above (13-15, 18, 19). This lends support both to the supposed porous, polymer-like nature of these oxide films as well as to the fact that the nature of the oxide film is different in the reduced and oxidized forms (reaction [1]), as was suggested originally by the marked asymmetry of the peaks in Fig. 1.

pH Dependence of oxide reaction.—One of the previously reported characteristics of hydrous oxide films formed at electrodes such as Ir (23) is their unusual pH dependence of greater than 60 mV/pH unit. This has been explained (23-26) as indicative of the different acid/base properties of the oxidized and reduced forms of the oxide, with the oxidized form of the metal sites within the film being more strongly complexed by hydroxide ions than the reduced form. The overall consequence of this is the requirement for counterions, *i.e.*, Na^+ in NaOH solutions, to be involved in the reaction in order to maintain charge neutrality within the oxide film.

The pH dependence of the hydrous oxide film formed in 1*M* NaOH solutions at amorphous Ni-Co alloys was tested with a relatively thin oxide film by transferring the electrode between solutions of different pH (between 12 and 14) but of identical ionic strength. Figure 6 demonstrates a series of voltammograms obtained in such experiments. Over this range of pH, the A_2 peak potential shifts negatively by 85-95 mV per pH unit, while C_2 moves negatively by only 70-80 mV. If the potentials of peaks A_2, C_2, and that midway between A_2 and C_2 are plotted *vs.* pH (Fig. 7), an overall 75-85 mV pH dependence is obtained.

A 90-mV pH dependence is equivalent to a 3:2 ratio of hydroxide ions (in alkaline solutions) to electrons, *i.e.*,

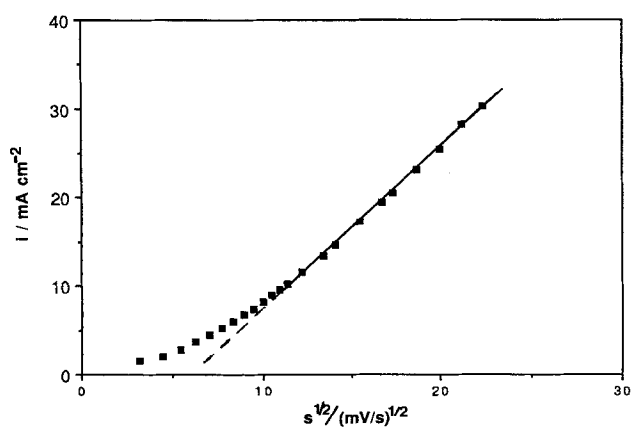

Fig. 5. Dependence of peak current density on $s^{1/2}$ for data of Fig. 4, right.

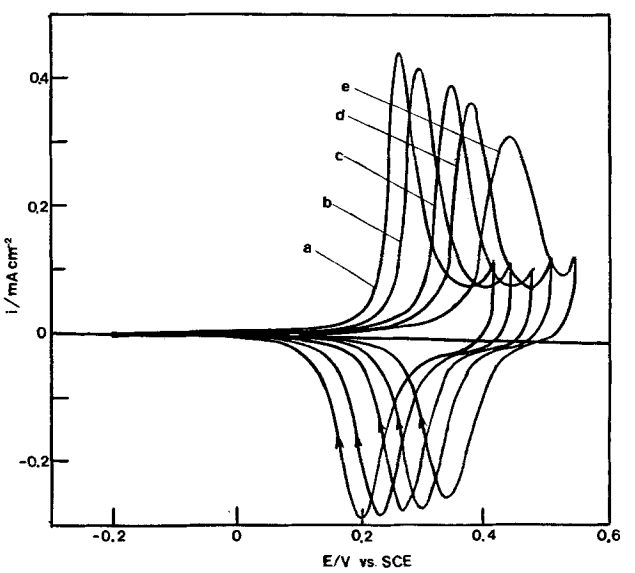

Fig. 6. CVs at 10 mV/s for oxide film formed by 60 min of potential cycling in 1M NaOH in solutions of pH 14 (a), 13.5 (b), 13 (c), 12.5 (d), and 12 (e).

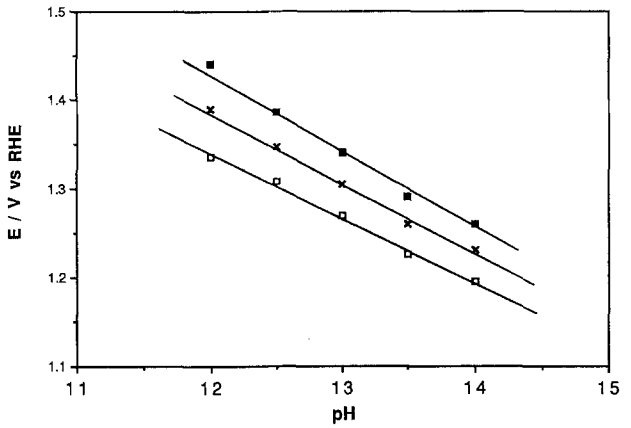

Fig. 7. Plot of potential of peak A_2 (■), C_2 (□), and midway between these (×) vs. pH; data taken from Fig. 6.

when two electrons are removed from the oxide film during oxidation, three hydroxide ions are injected. This process alone would result in a negatively charged film, and therefore, one Na^+ ion per three OH^- ions must also be incorporated during oxidation, *i.e.*

$$2[M(OH)_2 \cdot nH_2O) + Na^+ + 3\ OH^- \leftrightarrow M_2(OH)_7^- \cdot nH_2O \cdot Na^+ + 2e^- \quad [4]$$

The inferred involvement of Na^+ ions in the oxide reaction is strongly supported by the XPS determination of the composition of a typical oxide film, removed from the solution at E_+ when it would be assumed to contain Na^+ ions (reaction [4]). In addition to the expected presence of Ni, Co, Cr, Mo, and O (1), Fig. 8 shows substantial levels of Na throughout the oxide film. Although it cannot be ruled out that the Na is present simply in the form of excess electrolyte in the oxide film, it is likely that loosely bound solution would be lost in the high vacuum conditions of the instrument.

The presence of Na in the film is consistent with the identification of Li as a component of the oxidized form of Ir oxide films in LiOH solutions, as determined by the chemical extraction of the ionic content of the oxide film and its analysis by atomic spectroscopic methods (27), while no Li was found in the reduced form. In addition, there have been a number of reports of the presence of alkali metal ions in the oxidized form of Ni oxide films in battery studies (28). Also, the fact that Na is present in the oxidized form of the oxide (and its depletion after reduction, as implied from the observed pH dependence in Fig. 7) is consistent with the apparent difference in the nature of the oxidized and reduced forms of the oxide, as seen by their different electrochemical behavior (Fig. 1 and 2). The injection/removal of hydroxide and sodium ions during oxidation/reduction could be the diffusion-limited process observed for thick oxide films (Fig. 5).

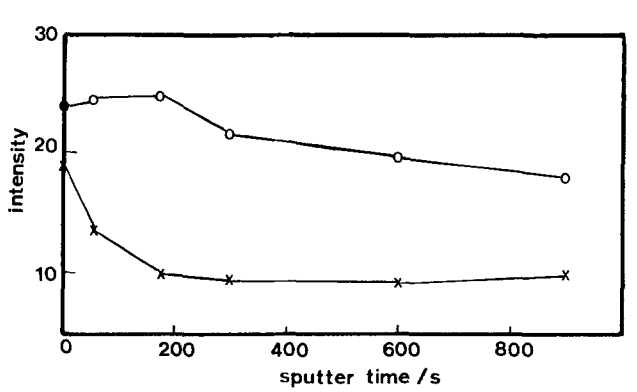

Fig. 8. XPS depth profile of Na (×) and O (○) in oxide film (CEF = 70) formed in 1M NaOH solution. Sputtering rate of film not known.

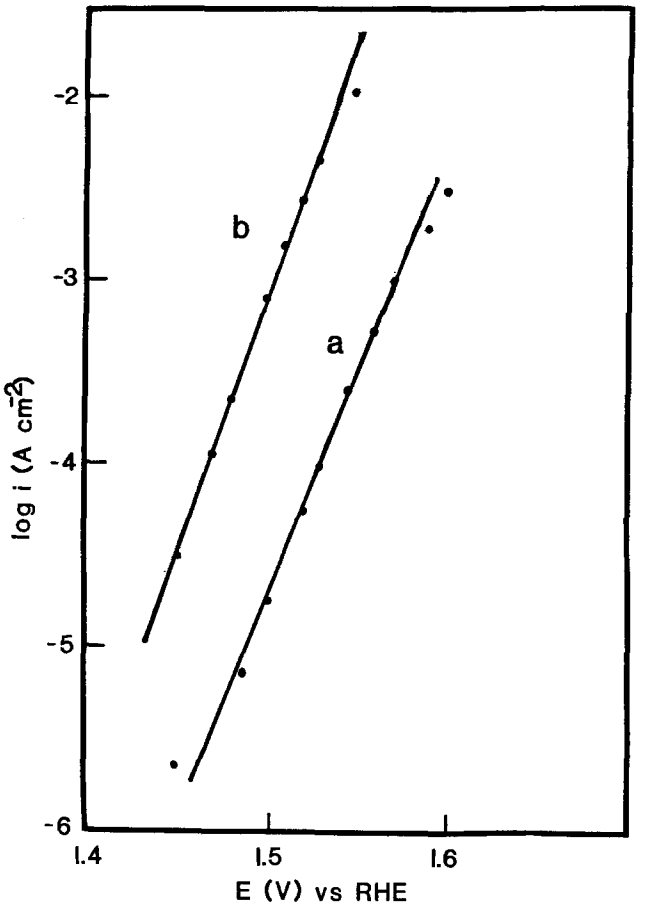

Fig. 9. Tafel plots for OER at (a) as-received alloy electrode and (b) oxidized alloy (CEF = 100).

There are several other interesting and possibly significant aspects to the data shown in Fig. 6 and 7. First, the buffering and supporting electrolyte have introduced other ions into the solution, which may also be involved in the charge compensation processes during oxidation/reduction of the oxide film, perhaps leading to a pH dependence of less than 90 mV. This may be the cause for the fact that at pH 12 (Fig. 6), the anodic and cathodic peaks are more symmetrical than at higher pH. Recalling the impact of film thickness and sweep rate on the potential of the anodic peak from Fig. 1, it is possible that changes in the solution composition could affect the degree of hydration of the oxide and hence its thickness, even for a constant charge density. Therefore, even though the CVs were recorded at the relatively slow sweep rate of 10 mV/s in Fig. 6, the above factors may introduce complications which cannot be controlled or fully accounted for.

Oxygen evolution at hydrous Ni-Co oxide films.—The rate of the OER at hydrous oxide-coated alloy electrodes was determined at constant potential in the range of 1.45 to 1.6 V, and compared to that observed at the as-received alloy surface and with data in the literature for Ni, Co, and various spinel oxide electrodes. Figure 9 shows that the Tafel slope of the OER at the hydrous Ni-Co oxide electrode is *ca.* 45 mV, as was also the case at the fresh electrode surface. At potentials greater than 1.6 V, a different slope develops, which is likely to be related to the onset of diffusion control.

A 40-mV Tafel slope has been reported previously for the OER at polycrystalline Ni (29-31), while 60 mV slopes are also sometimes observed (8, 30). At hydrous Co oxide surfaces, Tafel slopes of *ca.* 50-60 mV have been reported (8), while $NiCo_2O_4$ spinels appear to yield slopes of closer to 40 mV (30), suggested to reflect (32) oxygen evolution via the decomposition of a M(IV) oxide to the M(II) form, where M is either Co or Ni. Therefore, the 45 mV slopes shown in Fig. 9 indicate that the surface is behaving more like a Ni oxide or a spinel oxide electrode surface, rather

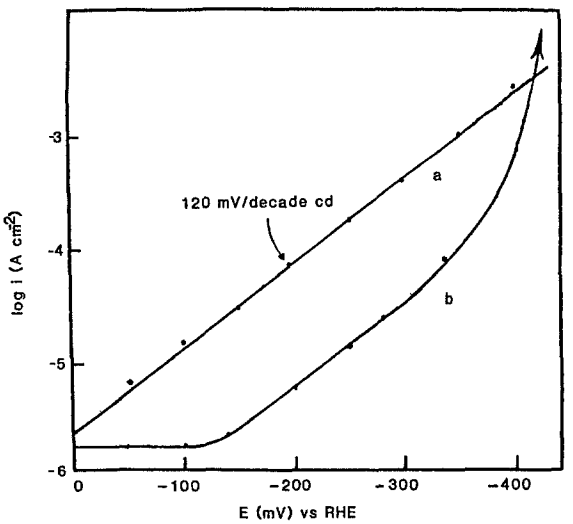

Fig. 10. Tafel plots for HER at (a) as-received Ni-Co amorphous alloy and (b) electrochemically formed oxide.

than like oxidized Co. This is consistent with the absence of other electrochemical evidence for Co oxide in this work (1).

It should be noted (although this is not shown in Fig. 9) that the OER currents are roughly in proportion to the film thickness, as gauged from the charge density in the A_2/C_2 peaks and the observed relationship (1) between charge density and dry film thickness, determined by SEM examination. Therefore, very high current densities can be achieved for the OER, both for this reason and due to the low Tafel slope. Also, the oxide film was found to be chemically and physically stable, remaining intact on the electrode surface throughout the OER experiments, and exhibiting no loss of activity.

The HER at oxidized amorphous Ni-Co alloy electrodes.—One of the pronounced effects of potential cycling of a fresh alloy electrode is the decrease in the rate of the HER with surface oxidation. To examine this more closely, a Tafel plot for the HER at an as-received alloy, which had never been subjected to positive potentials in alkaline solutions, is shown in Fig. 10. A Tafel slope of *ca.* 120 mV/decade of current density is seen in the potential range of 0 to −0.45 V *vs.* RHE. This value is very close to previously reported slopes at similar alloy and related metal surfaces in alkaline solutions (33-36), and indicates that the first electron transfer step is rate-determining. Extrapolation of the plot to 0.0 V gives an exchange current density of 2.5×10^{-6} A/cm^2, comparable to that at electrodes such as $Ni_{58}Co_{20}Si_{10}B_{12}$ (33).

The Tafel plot for the HER at an oxidized amorphous Ni-Co alloy is rather unusual (Fig. 10, curve b), in that three Tafel regions are observed. At overpotentials less than 150 mV, a steady-state current density of *ca.* 1.7×10^{-6} A/cm^2 is observed, while at higher overpotentials, a slope of 120 mV is seen, as at the original alloy surface. When the potential was extended to *ca.* −300 mV, the current density began to increase continuously with time at each potential, and a steady-state reading could not be obtained. Eventually, current densities greater than those at the fresh electrode surface were observed at these potentials.

It appears that at low overpotentials, the oxide film functions as a barrier to the HER, permitting only a low-rate, diffusion-controlled reaction to occur, perhaps at pores in the film. This could be viewed as an advantage in terms of the corrosion resistance of these alloys in alkaline solutions, in that the cathodic reaction would be severely hampered, but it is clearly a disadvantage in terms of the electrocatalysis of the HER. Once the overpotential exceeds a critical value, the first electron transfer step is again rate-determining, although the rate of the reactions is still much less than that at the fresh alloy surface. At still higher overpotentials, the continuous increase in the HER currents with time indicates that some form of oxide reduction and/or breakdown is occurring. Indeed, after time spent in this region of the Tafel plot, the next complete anodic scan shows relatively large currents due to the Ni to Ni(II) oxide (and Co to Co(II) oxide) conversion process, indicating that some reduction of oxide probably occurred at negative potentials, forming an active, high-area electrode surface.

Table I. Open-circuit potentials in chloride-containing solutions.

Electrode condition	E (V) *vs.* SCE
Polycrystalline Ni (as received)	−0.55
Ni-Co alloy	
As received	−0.11
Oxidized in 1*M* NaOH	
after 2 scans	−0.03
550 Å oxide	+0.17
1300 Å oxide	+0.45
1600 Å oxide	+0.52
6000 Å oxide	+0.55

Behavior of oxidized amorphous alloy in chloride solutions.—Preliminary experiments in near-neutral chloride solutions have focused on the resistance to oxidation of the amorphous Ni-Co alloy, both in the as-received and pre-oxidized state, and involved simply the monitoring of the OCP of the samples, which reached steady-state values after a few minutes of immersion in the solution. Table I (37) shows the measured OCP as a function of the thickness of the oxide film, formed by potential cycling in alkaline solutions (Fig. 1). It can be seen that the thicker the oxide film, the higher the OCP.

It has been previously reported (38-42) that the addition of Cr and/or the presence of both Cr and Mo in amorphous alloys is particularly effective in enhancing the corrosion resistance of these alloys. However, the results of Table I show that, under OCP conditions, the hydrous Ni-Co oxide films, from which Cr and Mo have been depleted, are more "noble" in character than the as-received Cr-enriched alloy surface. The hydrous oxide film may be a better barrier to chloride ions than is the thin Cr oxide film on the original surface.

Figure 11 shows the slow sweep CVs for both an as-received and a hydrous oxide-covered alloy electrode in *ca.* $10^{-2}M$ chloride solution (pH 9.6). Both of these CVs show the hysteresis typical of a pitting process. Also, a gel-like product could be observed near the electrode surface in both cases, reflecting the formation of soluble metal oxide species.

The pitting potential (E_p) observed for the hydrous oxide coated specimen is *ca.* 300 mV more positive than that of the unoxidized sample. However, both display a similar healing potential (E_h) in the negative-going scan. These results imply that the electrochemically formed oxide film serves as a barrier to chloride ions only at relatively low potentials. Once a critical potential is exceeded, it is reasonable to suggest that both hydroxide and chloride ions

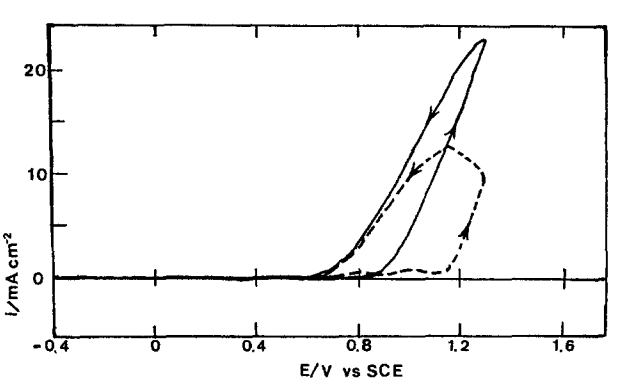

Fig. 11. CVs of as-received (——) and electrochemically oxidized (CEF = 85) alloy (---) in pH 9.6 solution with $2 \times 10^{-2}M$ NaCl; s = 2 mV/s.

may be injected into the film during oxidation, the chloride ions possibly being involved in charge compensation due to the low concentration of hydroxide in this solution and also being drawn into the oxide by the positive electrode potential. The presence of chloride inside the oxide film at positive potentials is then expected to cause metal dissolution.

Reactions [5] and [6] may represent two possible processes (of a range of feasible reactions) which may be involved in the oxidation/reduction of the Ni/Co hydrous oxide in these chloride-containing solutions

$$\text{M(II)oxide} \cdot n\text{H}_2\text{O} + 2\text{Cl}^- + \text{Na}^+ \leftrightarrow \text{M(III)oxide} \cdot n\text{H}_2\text{O} \cdot 2\text{Cl}^- \cdot \text{Na}^+ + e^- \quad [5]$$

$$2[\text{M(OH)}_2 \cdot n\text{H}_2\text{O}] + 2\text{Cl}^- + \text{Na}^+ + \text{OH}^- \leftrightarrow \text{M}_2(\text{OH})_5 \cdot 2\text{Cl}^- \cdot \text{Na}^+ \cdot n\text{H}_2\text{O} + 2e^- \quad [6]$$

The E_p and E_h values obtained with the hydrous oxide-coated specimens were reproducible in the subsequent potential scans. This may suggest that chloride ions are expelled from the oxide film during reduction in the cathodic scan, and reinserted in the subsequent anodic sweep, consistent with the proposed nature of the reaction of these hydrous oxide films.

It is noteworthy to recall that, during the HER study, the hydrous oxide film inhibited the HER at relatively low overpotentials, but that once a critical overpotential was reached, it no longer served as a barrier to this reaction. This is analogous to the situation in the presence of chloride ions since, in both cases, both ion and solvent injection/expulsion are involved during the reaction, and critical potentials are required to initiate the reaction.

Summary

The electrochemical response of hydrous oxide films, formed at a Ni-Co amorphous alloy by potential cycling, is characterized in cyclic voltammetric experiments by a single pair of peaks, centered at *ca.* 1.35 V. The anodic reaction is clearly more inhibited than the cathodic one, with the peak moving positively into the range of the OER with increasing sweep rate. The cathodic peak does not alter its position or shape significantly with sweep rate, and for thin oxide films, the reaction is kinetically reversible to relatively high sweep rates. Thicker films demonstrate diffusion-controlled kinetics, even at low sweep rates, similar to the behavior of other hydrous oxide materials and many polymer-modified electrodes, in which ion/solvent injection and expulsion processes are known to occur during the electrochemical reactions. This involvement of solution ions is consistent with the 75-80 mV pH dependence observed in this work, indicative of alkali metal injection during the oxidation step. It is probable that water also enters the oxide film during this process, so that the film can be viewed as swollen in the oxidized state and more compact after reduction.

The impact of the presence of the hydrous oxide film on the hydrogen and oxygen evolution reactions, as well as the resistance to chloride ions, was also investigated. The mechanism of the OER at bare and hydrous oxide-covered alloy electrodes appears to be the same (Tafel slope of 45 mV), although the rate of the reaction increases approximately in proportion to the amount of oxide film present. In contrast, the HER is greatly inhibited by the presence of the oxide film at low overpotentials, but at more negative potentials, the film appears to become reduced, resulting in the formation of a high-surface-area electrode. The oxide films also appear to protect the underlying metal from the effect of chloride ions, as seen by the substantial positive shift of the characteristic pitting potentials.

Acknowledgments

We gratefully acknowledge the support of this work by the Natural Sciences and Research Council of Canada. We also extend our thanks to Allied-Signal Corporation, for providing the glassy alloy samples, and to Dr. J. Brown, at CANMET/EMR, and Dr. D. Lloyd, at Alcan International Limited, for the XPS and AES analyses.

Manuscript submitted April 5, 1991; revised manuscript received June 20, 1991.

REFERENCES

1. K. Lian and V. I. Birss, *This Journal,* **138,** 2877 (1991).
2. L. D. Burke and T. A. M. Twomey, *J. Electroanal. Chem.*, **167,** 285 (1984).
3. L. D. Burke and D. P. Whelan, *ibid.*, **109,** 385 (1980).
4. D. N. Buckley and L. D. Burke, *J. Chem. Soc. Faraday Trans. 1,* **71,** 1447 (1975).
5. L. D. Burke and E. J. M. O'Sullivan, *J. Electroanal. Chem.*, **93,** 11 (1978).
6. L. D. Burke and E. J. M. O'Sullivan, *ibid.*, **117,** 155 (1981).
7. V. Birss, R. Myers, H. Angerstein-Kozlowska, and B. E. Conway, *This Journal,* **131,** 1502 (1984).
8. L. D. Burke, M. E. Lyons, and O. J. Murphy, *J. Electroanal. Chem.*, **132,** 247 (1982).
9. L. D. Burke and O. J. Murphy, *ibid.*, **109,** 373, 379 (1980).
10. S. Gottesfeld, J. D. E. McIntyre, S. Beni, and J. L. Shay, *Appl. Phys. Lett.*, **33,** 208 (1978).
11. S. Gottesfeld and J. D. E. McIntyre, *This Journal,* **126,** 742 (1979).
12. C. L. Ballestrasse, R. T. Ruggeri, and T. R. Beck, *Ann. Biomed. Eng.*, **13,** 405 (1985).
13. P. Daum and R. W. Murray, *J. Phys. Chem.*, **89,** 389 (1981).
14. P. J. Peerce and A. J. Bard, *J. Electroanal. Chem.*, **114,** 89 (1980).
15. P. Daum and R. W. Murray, *ibid.*, **103,** 289 (1979).
16. A. H. Schroeder, F. B. Kaufman, V. Patel, and E. M. Engler, *ibid.*, **113,** 193 (1980).
17. A. H. Schroeder and F. B. Kaufman, *ibid.*, 209.
18. H. Dahms, *J. Phys. Chem.*, **72,** 362 (1972).
19. C. R. Martin, I. Rubinstein, and A. J. Bard, *J. Am. Chem. Soc.*, **104,** 4817 (1982).
20. N. Oyama and F. C. Anson, *This Journal,* **127,** 640 (1980).
21. D. A. Buttry and F. C. Anson, *J. Am. Chem. Soc.*, **104,** 4824 (1982).
22. M. S. Wrighton, M. C. Palazzotto, A. B. Bocarsly, J. M. Bolts, A. B. Fischer, and L. Nadjo, *ibid.*, **100,** 7264 (1978).
23. P. G. Pickup and V. I. Birss, *This Journal,* **135,** 127 (1988).
24. L. D. Burke and T. A. M. Twomey, *J. Electroanal. Chem.*, **134,** 353 (1982).
25. D. E. Icenhower, H. B. Urbach, and J. H. Harrison, *This Journal,* **117,** 1500 (1970).
26. M. F. Yuen, I. Lawks, and W. C. Dautremont-Smith, *Solid State Ionics,* **11,** 19 (1983).
27. P. G. Pickup and V. I. Birss, *J. Electroanal. Chem.*, **240,** 171 (1988).
28. R. Barnard, G. T. Crickmore, J. A. Lee, and F. L. Tye, *J. Appl. Electrochem.*, **10,** 61 (1980).
29. J. P. Hoare, "The Electrochemistry of Oxygen," p. 277, Interscience, New York (1968).
30. J. Haenen, W. Visscher, and E. Barendrecht, *Electrochim. Acta,* **31,** 1541 (1986).
31. G. Bronoel and J. Reby, *ibid.*, **25,** 973 (1980).
32. P. Rasiyah and A. C. C. Tseung, *This Journal,* **129,** 1724 (1982).
33. G. Kreysa and B. Hakansson, *J. Electroanal. Chem.*, **201,** 61 (1986).
34. M. N. Hull, *ibid.*, **30,** app. 1 (1971).
35. M. Enyo in "Comprehensive Treatise of Electrochemistry," Vol. 7, B. E. Conway, J. O'M. Bockris, E. Yeager, S. U. M. Khan, and R. E. White, Editors, p. 263, Plenum Press, New York (1983).
36. M. A. V. Devanathan and M. Selvaratnam, *Trans. Faraday Soc.*, **56,** 1820 (1960).
37. K. Lian and V. I. Birss, in "Corrosion, Electrochemistry, and Catalysis of Metallic Glasses," (PV 88-1), R. B. Diegle and K. Hashimoto, Editors, pp. 220-231, The Electrochemical Society Softbound Proceedings Series, Pennington, NJ (1988).
38. C. J. Kasada, *Am. J. Sci.*, **22,** 131 (1931).
39. M. Naka, K. Hashimoto, and T. Masumoto, *J. Jpn. Inst. Met.*, **38,** 835 (1974).
40. T. Masumoto and K. Hashimoto, *Ann. Rev. Mater. Sci.*, **8,** 215 (1978).
41. Y. Waseda and K. Aust, *J. Mater. Sci.*, **1619,** 2337 (1981).
42. K. Cho, C-H. Hwang, C-S. Park, and Y-J. Ryeom, Proc. 4th Int. Conf. Rapidly Quenched Metals, 1467 (1982).